Tribol Lett (2011) 43:369–378
DOI 10.1007/s11249-011-9824-4

ORIGINAL PAPER

Atomic Friction Modulation on the Reconstructed Au(111) Surface

Qunyang Li · Yalin Dong · Ashlie Martini · Robert W. Carpick

Received: 17 March 2011 / Accepted: 2 July 2011 / Published online: 21 July 2011

Abstract Friction between a nanoscale tip and a reconstructed Au(111) surface is investigated both by atomic force microscopy (AFM) and molecular statics calculations. Lateral force AFM images exhibit atomic lattice stick–slip behavior with a superstructure corresponding to the herringbone reconstruction pattern. However, the superstructure contrast is not primarily due to variations in the local frictional dissipation (which corresponds to the local width of the friction loop). Rather, the contrast occurs primarily because the local centerline position of the friction loop is periodically shifted from its usual value of zero. Qualitatively, similar behavior is reproduced in atomistic simulations of an AFM tip sliding on the reconstructed Au(111) substrate. In both simulations and experiments, this centerline modulation effect is not observed on unreconstructed surfaces. Similarly, using a topographically flat surface as a hypothetical control system, the simulations show that the centerline modulation is not caused by variations in the reconstructed surface's topography. Rather, we attribute it to the long-range variation of the local average value of the tip-sample interaction potential that arises from the surface reconstruction. In other words, surface atoms located at unfavorable sites, i.e., in the transition between face-centered-cubic (FCC) and hexagonal-close-packed (HCP) regions, have a higher surface free energy. This leads to a varying conservative force which locally shifts the centerline position of the friction force. This demonstrates that stick–slip behavior in AFM can serve as a rather sensitive probe of the local energetics of surface atoms, with an attainable lateral spatial resolution of a few nanometers.

Keywords Nanotribology · Stick–slip · AFM · Friction mechanisms · Gold

1 Introduction

Despite the crucial role of friction in controlling the energy dissipation and wear [1] in small-scale engineering systems such as micro- and nano-scale mechanical systems, understanding and controlling friction at the nanometer scale remains a substantial challenge. One of the fundamental processes in nano-scale sliding is atomic stick–slip sliding. Theoretically predicted independently by Prandtl [2] and Tomlinson [3] (in a framework referred to as the "PT model"), atomic stick–slip friction was first observed by Mate et al. [4] using atomic force microscopy (AFM). It is caused by the local mechanical instabilities that occur when the downward gradient of the lateral tip-sample interaction force in the sliding direction approaches or exceeds the lateral stiffness of the system. The instability can be suppressed to enable smooth sliding with negligible dissipation via incommensurability [5], or by reducing [6], or oscillating [7] the load to avoid steep gradients in the lateral tip-sample interaction force. Transitions to multiple lattice-site slip [8, 9] and non-linear dynamical behavior [10] can also be observed. The stick–slip phenomenon enables imaging of the surface lattice of a broad range of materials [11], from graphene [12, 13] to self-assembled monolayers [14].

Q. Li (✉) · R. W. Carpick
Department of Mechanical Engineering and Applied Mechanics, University of Pennsylvania, Philadelphia, PA 19104, USA
e-mail: qli@seas.upenn.edu

Y. Dong · A. Martini
School of Mechanical Engineering, Purdue University, West Lafayette, IN 47907, USA

Most previous atomic stick–slip studies [15–17] have been focused on well-ordered, defect-free surfaces, where the interaction is a periodic function in space described by the two surface lattice vectors corresponding to the surface unit cell [18]. Therefore the "saw-tooth"-patterned variation of the lateral force along a given direction depends on a single length scale—the surface lattice periodicity in that direction. Recently, it was reported that atomic friction on certain surfaces with superstructures could exhibit interesting modulation effects: the local center position of the trace-retrace friction loops measured on graphene grown on SiC 81 substrate [19, 20], (referred to as the *centerline modulation* or sometimes as the *friction loop offset*) or the local amplitude (or half-width) of the trace-retrace friction loops measured on a KBr film deposited on a NaCl(001) substrate [20, 21], (referred to as the *amplitude modulation* or the *friction loop width*) could vary in concert with the underlying superstructures, as shown schematically in Fig. 1. It is noted that "local" here means a running average over a few stick–slip periods.

A centerline modulation can result from geometry, i.e., from a local slope of the surface [22], or can be the result of *friction asymmetry*, where the magnitude of the local friction force is different for forward (trace) and backward (retrace) scan directions [23–25]. The latter has been associated with the molecular tilt angle of monolayer films, which leads to an asymmetric mechanical response for shear forces [24]. In either case, the centerline modulation is a conservative effect: it does not affect the width of the friction loop, and thus there is no change in the energy dissipated during frictional sliding (which corresponds to the area enclosed by the friction loop). Alternatively, amplitude modulation involves a change in the amount of energy dissipated by friction.

Bennewitz and co-workers showed that the PT model can be modified to produce both of these friction modulation effects by considering phenomenological perturbations to the tip-sample interaction potential V as follows [19, 20, 26]:

$$V = V_{\text{lat}}\left(1 + \alpha \tilde{V}_1^{\text{sup}}\right) + \beta E_0 \tilde{V}_2^{\text{sup}}. \quad (1)$$

Here, E_0 is the amplitude of the original periodic tip-sample interaction potential V_{lat} (which could have a dependence on position x such as $V_{\text{lat}}(x) = E_0 \sin\left(\frac{2\pi x}{a}\right)$ where a is the lattice spacing), $\tilde{V}_1^{\text{sup}}$ and $\tilde{V}_2^{\text{sup}}$ are the non-dimensional modulation functions with long-range periods (much larger than the atomic spacing), and parameters α and β are the relative strength of the modulations. If $\tilde{V}_1^{\text{sup}}$ dominates $(\beta/\alpha \ll 1)$, then the amplitude of the friction loops will be locally modulated (Fig. 1a). As an example, using a one-dimensional model consisting of an elastic chain being dragged over a rigid substrate, Negri et al. recently showed that friction amplitude modulation could be caused by local mechanical softness and hysteresis at surface defects [27]. This also described friction force variations seen on ultrathin KBr films that had superstructures being deposited on the lattice-mismatched substrates [20]. If instead $\tilde{V}_2^{\text{sup}}$ dominates $(\alpha/\beta \ll 1)$, then the center position of the friction loops will be locally modulated (Fig. 1b). This was seen to apply well to the superstructures in graphene mono- and bi-layers on SiC [20]. Despite the apparent consistency with experiments, the

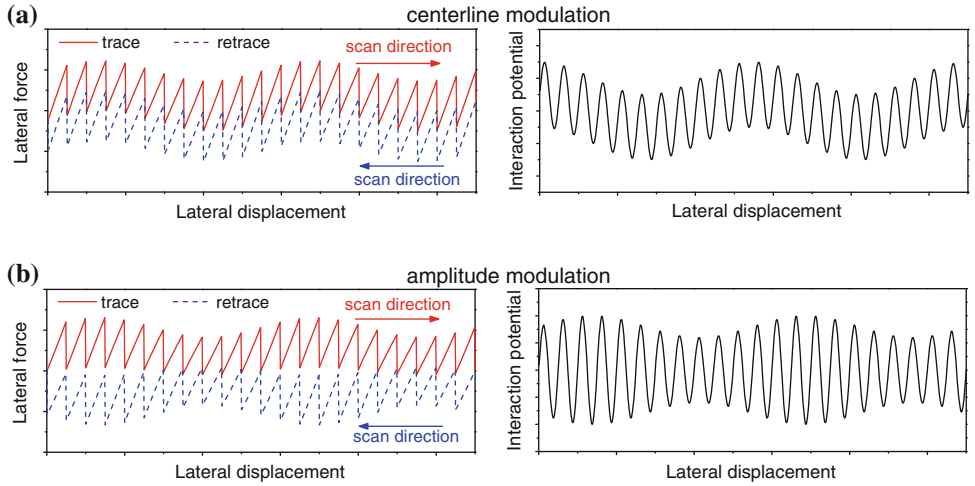

Fig. 1 Schematics of modulation effects in atomic stick–slip friction: **a** centerline modulation, where the local center (or mean) position of the trace-retrace friction loops varies in concert with the underlying superstructures; the corresponding interaction potential is shown on the right. The gradient of the long-range variation in the potential along the sliding direction corresponds to a varying conservative lateral force that, as shown in (**a**), shifts friction loop up and down. The largest shifts in the force corresponds to the largest gradients; and **b** amplitude modulation, where the local amplitude (or half-width) of the trace-retrace friction loops varies in concert with the underlying superstructure; the corresponding interaction potential is shown on the right

physical origins of these two types of modulations require further investigation.

Molecular simulation has evolved to be a very powerful tool for studying atomic stick–slip friction [28]. It has the advantage that it takes into account the position of every atom (and velocity, for dynamic simulations), which is impossible for reduced-order models like the PT model. Similarly, molecular simulations can capture the physical processes at the buried interface and within the surrounding material, which are rarely accessible to experiments. In addition, many more parameters can be altered and studied in molecular simulations, such as materials, orientations, geometries, surface reconstruction, and so on, to control conditions at the atomic level to validate ideas and isolate proposed mechanisms. Recently, we demonstrated that the energetics of the stick–slip behavior observed by AFM experiments can be well described by molecular dynamics simulations, provided that the simulated sliding speed is low enough [29], and that molecular statics provides a consistent description of the friction process in the low-temperature limit.

In this study, atomic stick–slip friction on a reconstructed Au(111) surface with a well-known superstructure is studied by AFM and molecular statics simulations. In experiments, we observe a clear centerline modulation in the lateral force whose structure is consistent with the Au(111) herringbone reconstruction. A qualitatively similar modulation effect is reproduced by molecular statics simulations on a rigid reconstructed Au(111) surface. The simulations confirm that the centerline modulation is caused by the surface reconstruction, because the modulation is absent on an unreconstructed surface, even when the scan direction is not along the close-packed direction of the Au(111) surface. More importantly, the simulations indicate that the modulation effect is not primarily due to any topography (slope) as previously suggested [20]; instead, it is due to long-range lateral variations of the interfacial potential which arise from the periodic transitions of Au surface atoms between face-centered-cubic (FCC) and hexagonal-close-packed (HCP) domains.

2 Experimental Results

Friction measurements were conducted using a RHK-UHV350 AFM operated in contact mode. A silicon cantilever with its tip coated by silicon nitride (CSC38 from MikroMasch) was used as the force sensor. The probe has a nominal spring constant $k = 0.03$ N/m and a nominal tip radius $R \approx 20$ nm. During the experiments, the normal force was kept at a constant positive value (approximately 0.4 nN, with a pull-off force of approximately 1.3 nN, based on similar probes calibrated with the same system) via a feedback system. The lateral force was continuously recorded during scanning. The reconstructed Au(111) surfaces were prepared by thermally evaporating 150 nm thick Au films onto freshly-cleaved mica disks (Ted Pella, Inc.) under high vacuum conditions (1×10^{-7} Torr). Films were then annealed with a hydrogen flame in air and immediately introduced into the AFM chamber. To desorb surface contaminants, films were briefly re-heated to $\sim$400°C under vacuum (1×10^{-6} Torr) right before the measurements. After heating, the chamber was back-filled, and continuously purged with the clean, dry nitrogen vapor from a liquid nitrogen dewar. All measurements were performed at room temperature.

Depending on the annealing time and temperature, we find that the Au(111) surfaces exhibit different degrees of reconstruction. Higher annealing temperatures and longer annealing periods tend to produce surfaces with a higher density of reconstructed areas [30]. Figures 2a and b show two AFM lateral force images of a typical reconstructed surface. As highlighted by the black dotted lines, the variation of lateral force exhibits a herringbone pattern similar to the well-known $\mathrm{Au}(111) - (23 \times \sqrt{3})$ reconstruction. The Au(111) reconstruction has been previously observed experimentally by helium atom diffraction [31] as well as by scanning tunneling microscopy (STM) [32]. It is known to originate from two competing aspects [33]: (i) the surface atoms have a preferential bond length shorter than that in bulk due to their lower coordination; and (ii) the surface atoms are confined by the atoms below, where they prefer to sit on local potential minima (hollow sites). The competition leads to a configuration with two different close-packed domains, i.e., FCC (with ABC stacking, $\sim$3.9 nm wide), and HCP (with ABA stacking, $\sim$2.7 nm wide), periodically distributed on the surface. The orientation of these domains then alternates in a zigzag or herringbone manner, as schematically shown in Fig. 2c. The periodic transition from FCC to HCP sites is indeed confirmed in the atomically-resolved lateral force image in Fig. 2b by periodic shifts in atomic rows, consistent with previous observations [20]. This also demonstrates that a lateral spatial resolution approaching a small number of lattice sites has been attained in these experiments.

To better illustrate the atomic variation of friction, a line profile is shown in Fig. 3a for the trace (forward, or left to right) direction. Stick–slip events can be clearly recognized from the lateral force data. As suggested by the raw data, the total lateral force F_{lat} can be regarded as a sum of two components: one has a higher frequency corresponding to the short-range atomic stick–slip period, $F_{\mathrm{lat}}^{\mathrm{short}}$, the other has a lower frequency corresponding to the long-range modulation, $F_{\mathrm{lat}}^{\mathrm{long}}$. To highlight the influence of the

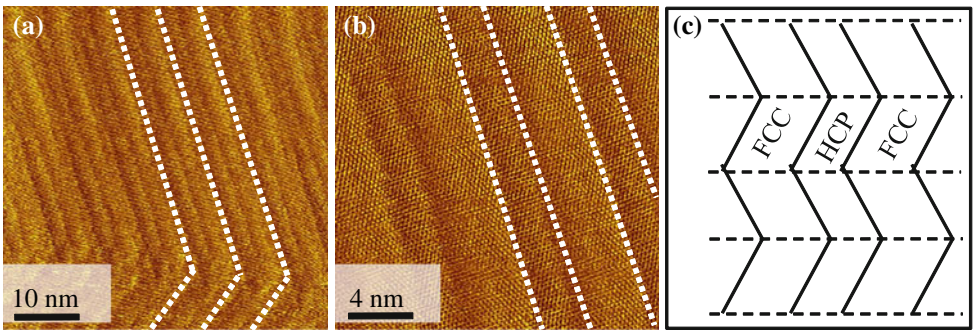

Fig. 2 AFM lateral force images of a reconstructed Au(111) surface at **a** a 50 nm scan size, **b** a 20 nm scan size, **c** A schematic of the Au(111) herringbone reconstruction showing two domains with different atomic stacking (FCC and HCP). Scan directions are from left to right in (**a**) and (**b**). The *dotted lines* are drawn to highlight the pattern of the friction variation. The atomic lattice is resolved in (**b**)

long-range superstructure due to the reconstruction, (i.e., $F_{\text{lat}}^{\text{long}}$), we applied a low-pass Fourier filter with a 2 nm cut-off period to the raw lateral force data so that the local high-frequency atomic stick–slip variation, (i.e., $F_{\text{lat}}^{\text{short}}$) is suppressed. The filtered data essentially represents the local mean value of the raw stick–slip curves averaged over a few stick–slip periods. The filtered lateral force data, the red solid curve in Fig. 3a, varies as the tip slides over the reconstructed surface. The same variation occurs for scanning in the retrace (right to left) direction as well, in phase with the variation in the forward direction (blue dashed curve in Fig. 3b). This means that the centerline of the friction loops (the local average of the trace and retrace lateral forces) is varying substantially (Fig. 3c, green solid curve), while the variation in friction (half the difference between the trace and retrace lateral forces or half-width of the friction loops, Fig. 3c, orange dashed curve) is much less significant. This centerline modulation effect is more obvious in the low-pass filtered 2D lateral force images, shown in Figs. 3d and e for the trace and retrace directions, respectively, where the variations are nearly in phase for both trace and retrace scan directions. The variation of the filtered lateral force exhibits essentially the same pattern as the reconstruction, demonstrating that there is a direct relation between the two.

It is noted that both *amplitude modulation* [19, 20] and *centerline modulation* [20, 21] will lead to variations of the local averaged lateral force. However, for amplitude modulation, the variations for trace and retrace curves will have *opposite* phases (i.e., maxima in the long-range variation of the trace curve are minima for the retrace curves); while for centerline modulation, the variations will have the *same* phase (i.e., peak local averaged lateral forces occur at the same location for the trace and the retrace). As seen in the friction loop in Fig. 3b, and in the full lateral force images shown in Figs. 3d and e, the contrast for the trace and the retrace lateral force measurements is in phase, clearly demonstrating that the observed modulation is primarily a centerline modulation, not an amplitude modulation. Because the lateral force of the trace and retrace curves vary nearly in concert with one another, the local frictional dissipation (the area enclosed between trace and retrace curves) is relatively constant.

Recently, a long-range variation in the lateral force image was reported for the reconstructed Au(111) surface by Steiner et al. [20]. The data that was shown for the forward scan direction only, exhibited a "tilted" appearance over several atomic periods. In other words, there was an overall slope to the filtered lateral force data. This tilt, which could be an example of centerline modulation, was proposed to be caused by variations in the local slope of the surface due to topographic height changes of the reconstructed surface. In the present experiments, the peak-to-peak amplitude of the long-range centerline modulation is approximately 0.5 nN, which is 1/4 to 1/5 of the local stick–slip amplitude. The height variation on the reconstructed Au(111) surface is only 0.015 nm [31], and the external normal load is rather small ($\sim$0.4 nN). The expected lateral force fluctuation due to topographic slope [22] will then be only a few picoNewtons. This is over 10 times smaller than our experimental observations (we assume a typical lateral force constant—roughly 14 pN/signal unit—calibrated for similar AFM cantilevers on the same AFM system).

Thus, something other than local topographic slopes must contribute to this long-range centerline modulation. Variation of the lateral force due to surface reconstruction was also observed by Nie et al. [34] for an AFM tip sliding over reconstructed gold surface in air. Although the authors did not specify the type of modulation, they proposed that the variation was caused by variation of the potential corrugation, rather than the reconstructed surface's topography. This mechanism is explored further in the next section.

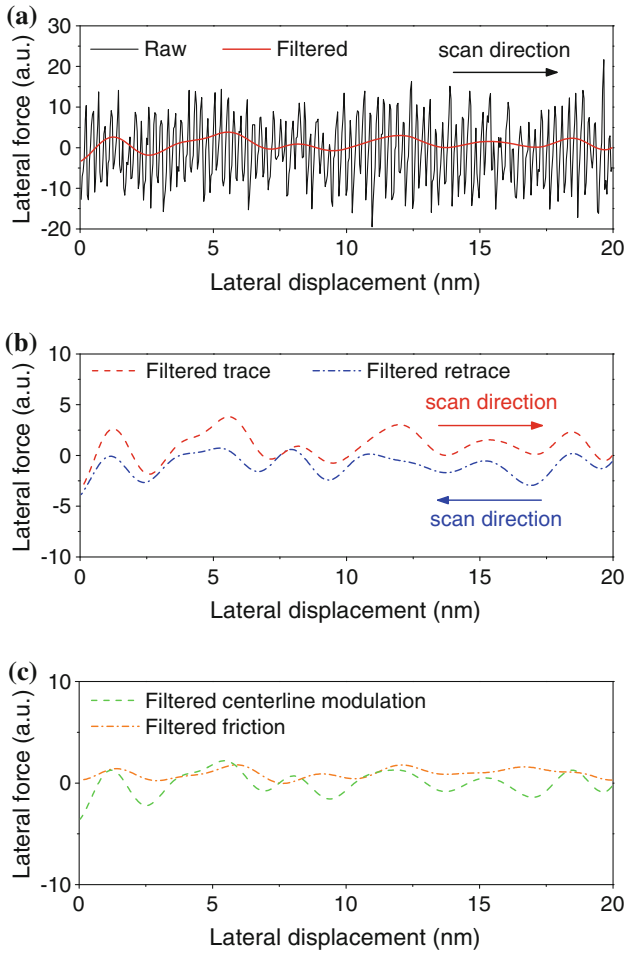

Fig. 3 **a** Line profiles showing both the raw experiment and the low-pass filtered lateral force signal (trace direction). **b**, **c** The low-pass filtered data for: **b** trace and retrace signals, and **c** centerline and half difference (friction) of the trace and retrace signals. **d**, **e** Low-pass filtered AFM lateral force images highlighting the centerline modulation effect: **d** trace (left to right), and **e** retrace (right to left). The contrast is clearly in phase, showing that the variations are primarily due to local centerline modulation, not varying friction

3 Simulations and Discussions

To further explore other mechanism(s), we carried out molecular statics simulations to model an AFM tip sliding against various Au(111) surfaces. In the simulations, we chose the tip material to be platinum because: (a) in the experiments, we observed qualitatively similar friction behavior on reconstructed Au(111) when using a platinum-coated tip, just with a poorer contrast (possibly due to the spring constants of the cantilever used); and (b) we have recently demonstrated a model [29] to describe Pt–Au interatomic interactions, which is more reliable than the complicated interactions between silicon nitride (amorphous, likely to have unknown stoichiometry that includes some O and also –OH groups) and Au. Although this choice of model tip material is made for reliability and convenience, the results should be generally applicable, since the friction variation we are studying is dominated by the larger scale reconstruction of the substrate, not the atomic structure of the tip. The platinum tip in the simulation is a truncated cone having (111) surface termination with an area of 7.23 nm^2 (91 atoms). Since commensurate contact between the tip and the substrate is unlikely to occur in the experiments (both for Pt–Au and Si_3N_4–Au cases), the orientation of the tip is rotated 30° in-plane to avoid quasi-commensurability (Pt and Au have only slightly different lattice constants) as shown in Fig. 4a.

Voter-Chen style Embedded Atomic Method (EAM) potentials are employed for all interatomic interactions, where the cross potential is the arithmetic mean of the interaction parameters for the pure materials with a re-scaled electron density function, such that there is a single summed electron density [35]. Considering the large unit cell size of the reconstruction, molecular statics instead of molecular dynamics is implemented to simulate the friction process, which can significantly reduce computation time at the expense of observing dynamical effects. This choice is justified by our verification that Pt–Au contacts exhibit well-behaved single slips in the thermally-activated regime [29]. The treatment of atoms in simulations is briefly described below. The three layers of

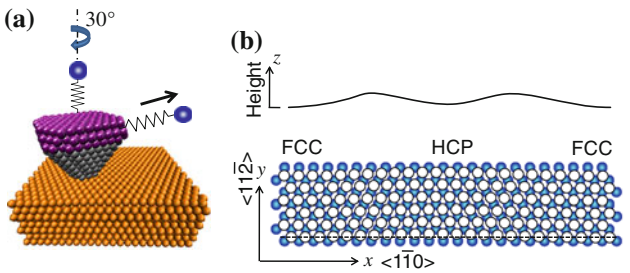

Fig. 4 **a** The simulation model of a Pt tip sliding over a gold substrate. **b** A schematic showing the atomic configuration of the reconstructed Au(111) surface: *black/white* circles represent the atoms from the top layer and *blue* spheres represent those from the second layer. *black/white* circles on the left-hand-side sit on FCC sites (ABC stacking), and they gradually shift to HCP sites (ABA stacking) in the middle region, and then they gradually shift back to FCC sites on the right-hand-side region. The *upper line* profile shows the height variation (rumpling) of the reconstructed surface (Color figure online)

the tip furthest from the interface are treated as rigid bodies. The model system also includes virtual atoms that do not experience inter-atomic interactions, but are coupled one by one to individual Pt atoms in the top three layers of the tip through harmonic loading springs as shown in Fig. 4a. The virtual atoms and springs, therefore, mimic the motion and stiffness of the AFM cantilever. The atoms are given freedom of movement in the direction perpendicular to the interface such that a given applied normal load (0 nN is used in the simulations) can be maintained. For each data point from the simulation, the virtual atoms are translated laterally at 15° with respect to the $[1\bar{1}0]$ direction with a distance of 0.01 nm, and the energetically relaxed configuration of unconstrained atoms is found using the L-BFGS minimization algorithm [24].

Conventional EAM potentials are unable to generate the Au(111) surface reconstruction. It has been suggested that this arises because these potentials, which are usually fitted to bulk material properties, underestimate the potential curvature for atoms close to the surface [36]. In our simulation, the reconstructed structure is imposed by manually positioning the gold atoms of the substrate according to the known reconstruction configuration and fixing their positions. Atoms in a perfect Au crystal have an FCC structure with an ABC stacking sequence of planes. In the presence of the reconstruction, some atoms on the surface relocate to new positions corresponding to a HCP structure, i.e., to a position corresponding to ABA stacking. Figure 4b shows a single period of the $\mathrm{Au}(111)-(23\times\sqrt{3})$ reconstruction with its alternating FCC and HCP domains. The periodic transition (from FCC to HCP and then back to FCC) results in an extra atom in the uppermost layer in each period. The atoms in the upper layer shift from their perfectly ordered FCC positions both in x (along the $<1\bar{1}0>$ direction) by an amount u^{shift}, and y (along the $<11\bar{2}>$ direction) by an amount v^{shift}. The shifts can be described by the soliton expression suggested by Harten et al. [31]

$$u^{\mathrm{shift}}(X)=\frac{2}{\pi}\arctan\left[\exp\left(\frac{X}{\Delta S}\right)\right]\cdot u^{\mathrm{FH}}, \tag{2}$$

$$v^{\mathrm{shift}}(X)=\frac{2}{\pi}\arctan\left[\exp\left(\frac{X}{\Delta S}\right)\right]\cdot v^{\mathrm{FH}}, \tag{3}$$

where $2\Delta S=1.18$ nm which is the half-width of the transition region bound by both the FCC and HCP domains, and $u^{\mathrm{FH}}=0.144$ nm and $v^{\mathrm{FH}}=0.083$ nm are the displacement shifts in the x and y directions when an atom moves from a perfect FCC site to a perfect HCP site. In addition to the lateral shifts, the reconstructed surface also rumples in the z direction (perpendicular to the Au(111) surface). The rumpling can be described by a Gaussian,

$$Z(X)=H\exp\left[-\frac{1}{2}\left(\frac{X}{\Delta S}\right)^2\right], \tag{4}$$

with height $H=0.015$ nm.

Figure 5a shows the lateral force versus lateral displacement obtained from simulations of scans on the reconstructed surface with relatively compliant loading springs (total lateral spring constant $k_{\mathrm{spr}}=22$ N/m). This leads to a total lateral stiffness (the slope of the lateral force with respect to the lateral displacement) of 12.0 ± 0.6 N/m (the reduction in stiffness is due to compliance of the tip, the contact, and the interface). The experimental value is 17.0 ± 0.9 N/m. As with the experimental data in Fig. 3, we applied a low-pass filter to the raw simulation data to highlight the influence of the relatively long-range superstructure from the reconstruction (red solid line in Fig. 5a). For a clearer comparison, the filtered curves (red solid curve and blue dashed curve for trace and retrace, respectively) are plotted in Fig. 5b together with the height profile (black dash-dot curve). The side-by-side comparison demonstrates that the filtered trace and retrace scans have a significant degree of coherence.

The centerline modulation effect is shown more clearly in Fig. 5c by the filtered centerline modulation curve (green solid curve), which is consistent with the experimental observations. In Fig. 5b, there are some regions where the variations of the filtered trace and retrace curves are slightly out of phase, which leads to some variation in the filtered friction curve in Fig. 5c. The system potential energy relative to its mean value as a function of the lateral displacement is shown as blue circles in Fig. 5d. In addition to the local atomic fluctuations, the potential clearly exhibits a long-range variation due to the surface reconstruction. This variation in potential energy is expected to lead to the centerline modulation of the lateral force, as shown in Fig. 1b. Indeed, as seen in Fig. 5e, where the gradient of the total potential energy along the sliding direction, with a low-pass filter is applied, is plotted with the centerline modulation from the simulation. The two are very well correlated.

While the simulation agrees with the experiment in showing that a centerline modulation effect occurs, the friction modulation seen in the simulation is larger than in the experiments. This may be attributed to the differences in energetics (which will occur, because the tip material is different than in the experiment), contact area, scanning speed, and inertia [29]. It may also be due to the different relative system compliances in the experiments and the simulations. Previous studies [6, 8, and 37–39] showed that frictional dissipation can strongly depend on the compliance of the loading system: stiffer systems give lower frictional dissipation. To investigate this, we performed

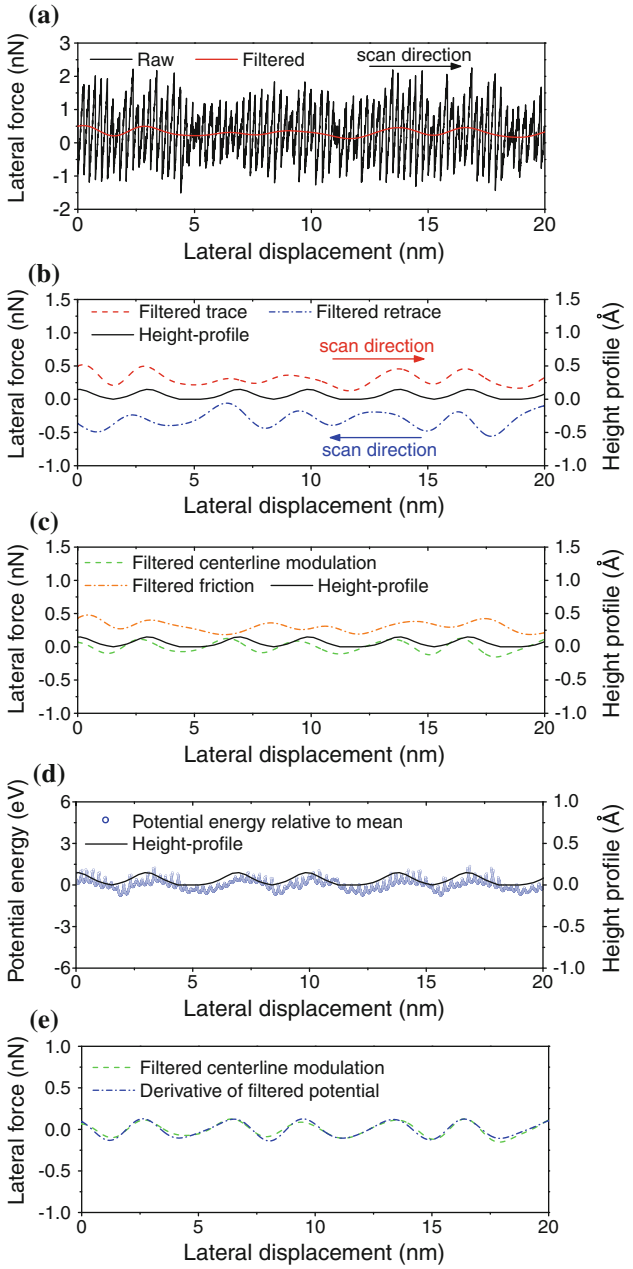

Fig. 5 **a** Lateral force versus lateral displacement data from simulations on the reconstructed Au(111) surface with relatively compliant loading springs: *black* curve for raw data, *red* curve for low-passed filtered data. **b** The low-pass filtered lateral force signal for trace (*red dashed curve*) and retrace (*blue dash-dot curve*) directions. **c** The filtered centerline modulation (*green dashed curve*) and friction (*orange dash-dot curve*) curves are also plotted side-by-side with the surface height profile (*black solid curve*). **d** The potential energy relative to its mean value (*blue circles*) is plotted side-by-side with the surface height profile (*black solid curve*). Topographically higher atoms, found on bridge sites in the HCP-FCC transition regions, are correlated with higher potential energy. **e** The gradient of total potential energy (low-pass filtered) along the lateral displacement direction (*blue dash-dot curve*), and the centerline modulation from (**c**) (*green dashed curve*) are highly correlated (Color figure online)

another set of simulations with much stiffer loading springs (total lateral spring constant $k_{spr} = 5000$ N/m; total lateral stiffness 19 N/m). The results are shown in Fig. 6. As expected, for simulations with a stiffer loading system, atomic stick–slip is substantially reduced (see Fig. 6a), and the lateral force signals for trace and retrace scans almost overlap with each other (see Fig. 6b). Therefore, the frictional dissipation and its variation are extremely small as depicted by the filtered lateral force curve (orange dash-dot curve) in Fig. 6c. In contrast to the diminishing friction, the variation of the centerline position is not sensitive to the system compliance, and it remains nearly as large as the calculations with the compliant loading system (see Figs. 6b, c). Both the experiment and the simulations yield a similar periodicity for the centerline modulation (about 6.8 nm, estimated from the peaks of autocorrelation function of the filtered lateral force signals).

The similarity in periodicity between the centerline modulation and the reconstruction superstructure

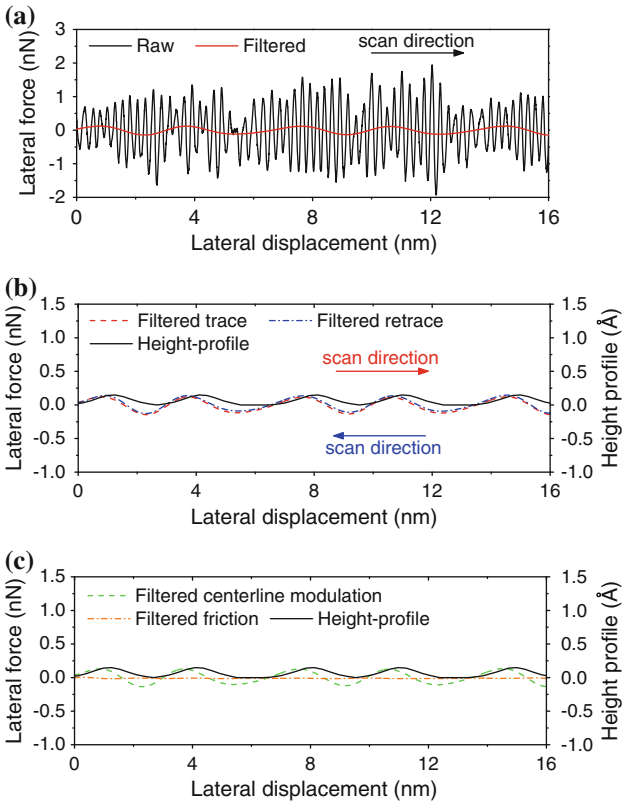

Fig. 6 **a** Lateral force versus lateral displacement curves obtained from simulations on the reconstructed Au(111) surface with stiff loading springs: *black* curve for raw data, *red* curve for low-passed filtered data. **b** The low-pass filtered lateral force signal for trace (*red dashed curve*) and retrace (*blue dash-dot curve*). **c** The filtered centerline modulation (*green dashed curve*) and friction (*orange dash-dot curve*) curves are also plotted side-by-side with the surface height profile (*black solid curve*) (Color figure online)

demonstrates that the modulation is caused by the surface reconstruction. This is confirmed by the fact that no clear centerline variation can be resolved when we run a simulation with an unreconstructed Au(111) surface, as shown in Fig. 7. Here, the small local amplitude variations of lateral force signals in Fig. 6a occur because the tip scan direction is at 15° with respect to the close-packed <1$\bar{1}$0> direction. In this case, the friction force can have a component in the surface plane that is perpendicular to the lateral direction [11]. Therefore, the lateral force at which the tip slips (the component of the static friction force in the lateral direction) will vary due to the misalignment of the sliding direction with the close-packed direction. However, this modulation effect due to misalignment does not affect the centerline position of lateral force signals appreciably, as indicated by Figs. 7b and c.

We also confirmed in the simulations that the lateral force centerline modulation is invariant to translation in the y (<11$\bar{2}$>) direction. This is shown in Fig. 8 by three sets

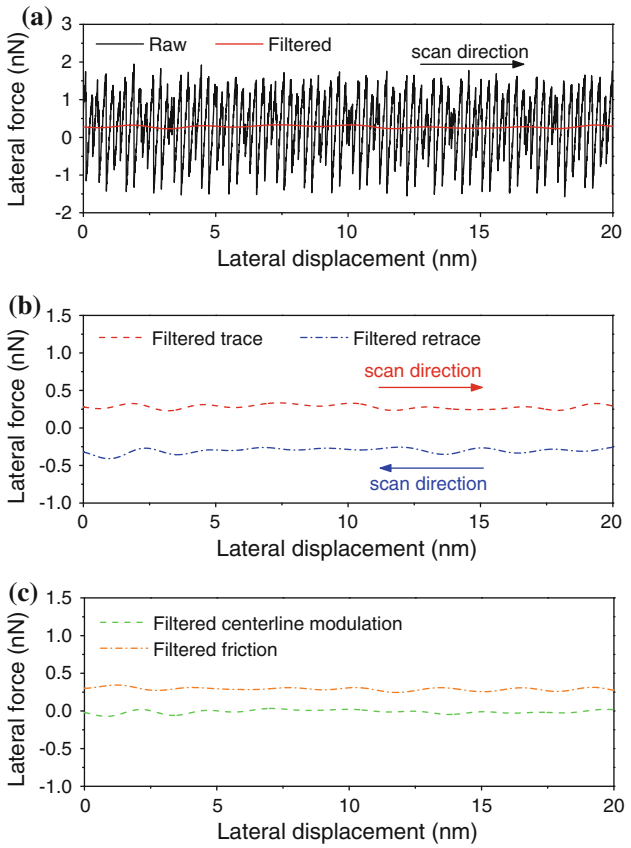

Fig. 7 **a** Lateral force versus lateral displacement curves obtained from simulation on the unreconstructed Au(111) surface with compliant loading springs: *black* curve for raw data, *red* curve for low-passed filtered data. **b** The low-pass filtered lateral force signal for trace (*red solid curve*) and retrace (*blue dashed curve*). **c** The filtered centerline modulation (*green solid curve*) and friction (*orange dashed curve*) curves are also plotted side-by-side with the surface height profile (*black dash-dot curve*) (Color figure online)

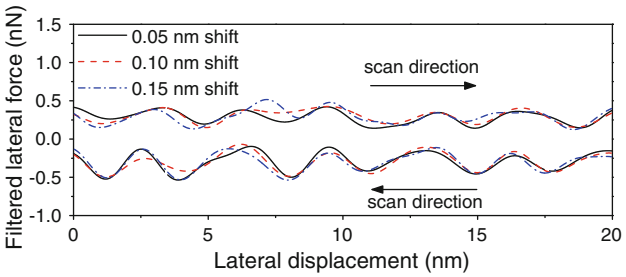

Fig. 8 Three sets of lateral force versus lateral displacement curves obtained from simulation with different shifts in the y (<11$\bar{2}$>) direction

of filtered trace-retrace lateral force curves where the y position has been shifted by 0.05 nm, 0.1 nm, and 0.15 nm. This again is consistent with the experimental observations.

Thus, the centerline modulation effect is seen to be correlated with the lateral gradient of the tip-sample potential. However, the variation of this gradient also matches the variation of the local topographic slope of the surface. To check for any contribution of topography to the lateral force modulation, we carried out another simulation on a "modified" reconstructed surface. The modified surface had a lateral configuration identical to the normal reconstruction as specified by Equations 2 and 3, but the height rumpling is deliberately suppressed to be zero. The lateral force variation on such a modified reconstructed surface is shown in Fig. 9. Although the surface is now atomically flat, we can still see a clear centerline modulation in lateral force signals with a similar magnitude as that exhibited by a rumpled surface. Similarly, the friction modulation is again highly correlated with the gradient of total potential energy, as shown in Fig. 9d. Therefore, we conclude that the centerline modulation on a reconstructed Au(111) surface is not primarily induced by the topographic slope variations, but rather it is caused by the long-range variation in the local average value of the interaction potential between the tip atoms and the reconstructed substrate atoms.

From the centerline modulation curve shown in Figs. 5c and e as well as Figs. 6c and 9c, and the discussions and control experiments discussed above, we can conclude that, in addition to the atomic variations, the tip-sample interaction potential is locally shifted to higher magnitude at the transition regions and to lower magnitude at the ordered (FCC or HCP) regions. The gradient of this long-range variation of the tip-sample interaction potential results in a conservative force that shifts the centerline value of lateral force as shown in Figs. 1a and 5e, and this shift is superposed with the lateral force variations due to atomic stick–slip behavior.

The long-range variation of the interfacial potential is not caused by topography; rather, it is governed by the

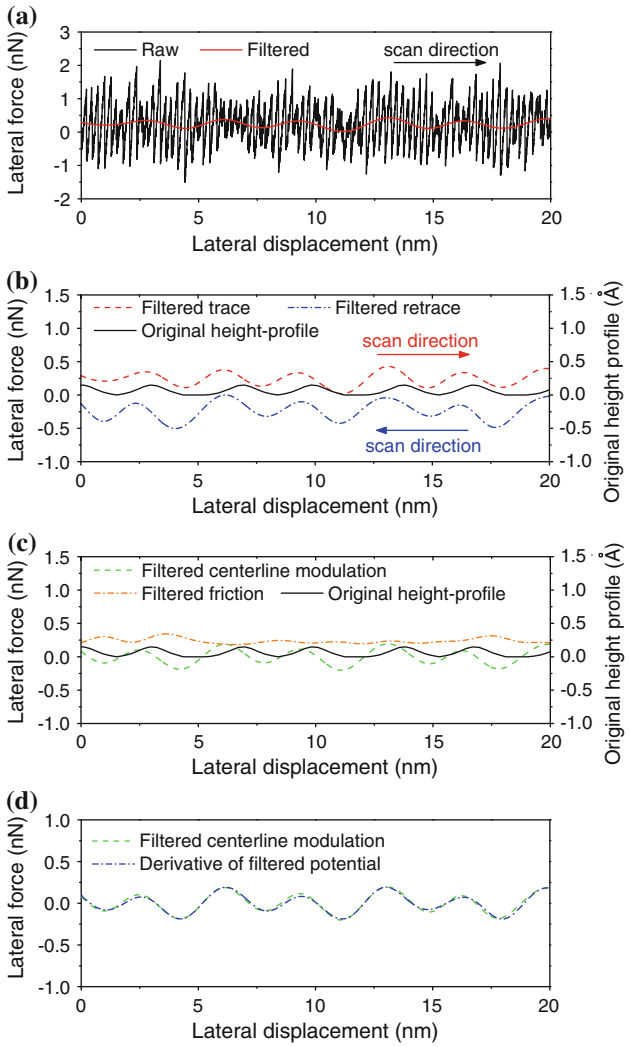

Fig. 9 **a** Lateral force versus lateral displacement curves obtained from simulation on a modified reconstructed surface that is atomically flat, i.e., where the height rumpling is deliberately suppressed with compliant loading springs: *black* curve for raw data, *red* curve for low-passed filtered data. **b** The low-pass filtered lateral force signal for trace (*red dashed curve*) and retrace (*blue dash-dot curve*). **c** The filtered centerline modulation (*green dashed curve*) and friction (*orange dash-dot curve*) curves are also plotted side-by-side with the original surface height profile (*black dash-dot curve*). **d** The gradient of total potential energy (*low-pass filtered*) along the lateral displacement direction (*blue dash-dot curve*), and the centerline modulation from (**c**) (*green dashed curve*) are highly correlated (Color figure online)

interaction between the tip atoms and the reconstructed substrate atoms in the contact zone. The magnitude of the variation will depend on the local commensurability and contact size, and further study is needed to explore these phenomena in full detail. However, it is clear that the bridge atoms in the transition regions between FCC- and HCP-stacked regions are in unfavorable sites, thus leading to modulations in the local surface free energy. This results in gradients (with respect to the lateral direction) in the long-range Fourier components of the tip-sample interaction potential, i.e., a force. This varying conservative force causes the variations in the local centerline of the friction loops observed here, and probably those reported elsewhere [19–21]. Unlike a friction force, whose direction changes depending on the sliding direction, the direction of this force is independent of sliding direction. It is thus an example of a locally varying friction asymmetry.

4 Conclusion

Atomically-resolved stick–slip friction between a nanoscale tip and a reconstructed Au(111) surface is studied both by AFM experiments and molecular statics simulations. The experiments show that the centerline position of the friction loops is periodically shifted by the surface reconstruction resulting in a herringbone pattern in the lateral force images. However, the net frictional dissipation does not vary appreciably with location. Qualitatively consistent behavior is reproduced by atomistic simulations only on the reconstructed Au(111) surfaces but not on unreconstructed surfaces. The behavior persists even if the small topographic variation of the surface atoms is suppressed. Thus, the centerline modulation is not caused by topographic variations of the reconstructed surface. Rather, it is caused by the long-range lateral perturbation in the local centerline value of tip-sample interfacial potential caused by the higher energy of atoms located in the unfavorable transition regions between HCP and FCC sites in the surface reconstruction. This suggests that stick–slip behavior in AFM can actually serve as a rather sensitive probe of the local energetics of surface atoms, with an attainable lateral spatial resolution of a few nanometers.

Acknowledgments This study was funded by the National Science Foundation under grants CMMI-0758604 & 0800154.

References

1. Mate, C.M.: Tribology on the Small Scale: A Bottom up Approach to Friction Lubrication and Wear. Oxford University Press, New York (2008)
2. Prandtl, L.: Ein gedankenmodell zur kinetischen theorie der festen körper. Z. Angew. Math. Mech. **8**(2), 85–106 (1928)
3. Tomlinson, G.A.: A molecular theory of friction. Philos. Mag. Series 7 **7**(46), 905–939 (1929)
4. Mate, C.M., McClelland, G.M., Erlandsson, R., Chiang, S.: Atomic-scale friction of a tungsten tip on a graphite surface. Phys. Rev. Lett. **59**(17), 1942–1945 (1987)
5. Dienwiebel, M., Verhoeven, G.S., Pradeep, N., Frenken, J.W.M., Heimberg, J.A., Zandbergen, H.W.: Superlubricity of graphite. Phys. Rev. Lett. **92**(12), 126101 (2004)
6. Socoliuc, A., Bennewitz, R., Gnecco, E., Meyer, E.: Transition from stick-slip to continuous sliding in atomic friction: entering a new regime of ultralow friction. Phys. Rev. Lett. **92**(13), 134301 (2004)

7. Socoliuc, A., Gnecco, E., Maier, S., et al.: Atomic-scale control of friction by actuation of nanometer-sized contacts. Science **313**(5784), 207–210 (2006)
8. Medyanik, S.N., Liu, W.K., Sung, I.H., Carpick, R.W.: Predictions and observations of multiple slip modes in atomic-scale friction. Phys. Rev. Lett. **97**(13), 136106 (2006)
9. Roth, R., Glatzel, T., Steiner, P., Gnecco, E., Baratoff, A., Meyer, E.: Multiple slips in atomic-scale friction: an indicator for the lateral contact damping. Tribol. Lett. **39**(1), 63–69 (2010)
10. Conley, W.G., Raman, A., Krousgrill, C.M.: Nonlinear dynamics in tomlinson's model for atomic-scale friction and friction force microscopy. J. Appl. Phys. **98**(5), 10 (2005)
11. Morita, S., Fujisawa, S., Sugawara, Y.: Spatially quantized friction with a lattice periodicity. Surf. Sci. Rep. **23**(1), 1–41 (1996)
12. Filleter, T., McChesney, J.L., Bostwick, A., et al.: Friction and dissipation in epitaxial graphene films. Phys. Rev. Lett. **102**(8), 086102 (2009)
13. Lee, C., Li, Q.Y., Kalb, W., et al.: Frictional characteristics of atomically thin sheets. Science **328**(5974), 76–80 (2010)
14. Lio, A., Charych, D.H., Salmeron, M.: Comparative atomic force microscopy study of the chain length dependence of frictional properties of alkanethiols on gold and alkylsilanes on mica. J. Phys. Chem. B **101**(19), 3800–3805 (1997)
15. Carpick, R.W., Salmeron, M.: Scratching the surface: fundamental investigations of tribology with atomic force microscopy. Chem. Rev. **97**(4), 1163–1194 (1997)
16. Dedkov, G.V.: Experimental and theoretical aspects of the modern nanotribology. Phys. Status Solidi A: Appl. Res. **179**(1), 3–75 (2000)
17. Gnecco, E., Bennewitz, R., Gyalog, T., Meyer, E.: Friction experiments on the nanometre scale. J. Phys. Condes. Matter **13**(31), R619–R642 (2001)
18. Steele, W.A.: Physical interaction of gases with crystalline solids. 1. Gas-solid energies and properties of isolated adsorbed atoms. Surf. Sci. **36**(1), 317–352 (1973)
19. Filleter, T., Bennewitz, R.: Structural and frictional properties of graphene films on SiC(0001) studied by atomic force microscopy. Phys. Rev. **B 81**(15), 155412 (2010)
20. Steiner, P., Gnecco, E., Filleter, T., et al.: Atomic friction investigations on ordered superstructures. Tribol. Lett. **39**(3), 321–327 (2010)
21. Maier, S., Gnecco, E., Baratoff, A., Bennewitz, R., Meyer, E.: Atomic-scale friction modulated by a buried interface: combined atomic and friction force microscopy experiments. Phys. Rev. **B78**(4), 5 (2008)
22. Ogletree, D.F., Carpick, R.W., Salmeron, M.: Calibration of frictional forces in atomic force microscopy. Rev. Sci. Instrum. **67**(9), 3298–3306 (1996)
23. Bluhm, H., Schwarz, U.D., Meyer, K.P.: Anisotropy sliding friction on the triglycine sulfate(010) surface. Appl. Phys. A: Mater. Sci. Process. **61**(5), 525–533 (1995)
24. Liley, M., Gourdon, D., Stamou, D., et al.: Friction anisotropy and asymmetry of a compliant monolayer induced by a small molecular tilt. Science **280**(5361), 273–275 (1998)
25. Hisada, K., Knobler, C.M.: Microscopic friction anisotropy and asymmetry related to the molecular tilt azimuth in a monolayer of glycerol ester. Colloid. Surf. A: Physicochem. Eng. Asp. **198**, 21–30 (2002)
26. Maier, S., Sang, Y., Filleter, T., et al.: Fluctuations and jump dynamics in atomic friction experiments. Phys. Rev. **72**(B24), 9 (2005)
27. Negri, C., Manini, N., Vanossi, A., Santoro, G.E., Tosatti, E.: AFM dissipation topography of soliton superstructures in adsorbed overlayers. Phys. Rev. **B81**(4), 5 (2010)
28. Szlufarska, I., Chandross, M., Carpick, R.W.: Recent advances in single-asperity nanotribology. J. Phys. D: Appl. Phys. **41**(12), 123001 (2008)
29. Li, Q.Y., Dong, Y.L., Perez, D., Martini, A., Carpick, R.W.: Speed dependence of atomic stick-slip friction in optimally matched experiments and molecular dynamics simulations. Phys. Rev. Lett. **106**(12), 4 (2011)
30. Nogues, C., Wanunu, M.: A rapid approach to reproducible, atomically flat gold films on mica. Surf. Sci. **573**(3), L383–L389 (2004)
31. Harten, U., Lahee, A.M., Toennies, J.P., Woll, C.: Observation of a soliton reconstruction of Au(111) by high-resolution helium-atom diffraction. Phys. Rev. Lett. **54**(24), 2619–2622 (1985)
32. Woll, C., Chiang, S., Wilson, R.J., Lippel, P.H.: Determination of atom positions at stacking-fault dislocations on Au(111) by scanning tunneling microscopy. Phys. Rev. **B39**(11), 7988–7991 (1989)
33. Narasimhan, S., Vanderbilt, D.: Elastic stress domains and the herringbone reconstruction on Au(111). Phys. Rev. Lett. **69**(10), 1564–1567 (1992)
34. Nie, H.Y., Mizutani, W., Tokumoto, H.: Au(111) reconstruction observed by atomic-force microscopy with lateral force detection. Surf. Sci. **311**(1–2), L649–L654 (1994)
35. Voter, A.F.: Los alamos unclassified technical report la-ur-93-3901 (1993)
36. Haftel, M.I.: Surface reconstruction of platinum and gold and the embedded-atom model. Phys. Rev. B **48**(4), 2611–2622 (1993)
37. Dong, Y.L., Perez, D., Voter, A.F., Martini, A.: The roles of statics and dynamics in determining transitions between atomic friction regimes. Tribol. Lett. **42**(1), 99–107 (2011)
38. Muser, M.H., Urbakh, M., Robbins, M.O.: Statistical mechanics of static and low-velocity kinetic friction. Adv. Chem. Phys. **126**, 187–272 (2003)
39. Shimizu, J., Eda, H., Yoritsune, M., Ohmura, E.: Molecular dynamics simulation of friction on the atomic scale. Nanotechnology **9**(2), 118–123 (1998)